

BIOPHYSICS

Protein condensates as aging Maxwell fluids

Louise Jawerth^{1,2}, Elisabeth Fischer-Friedrich^{3,4}, Suropriya Saha^{1*}, Jie Wang^{2†}, Titus Franzmann^{2,4}, Xiaojie Zhang⁵, Jenny Sachweh^{5‡}, Martine Ruer², Mahdiye Ijavi^{2§}, Shambaditya Saha⁶, Julia Mahamid⁵, Anthony A. Hyman^{2,3,7¶}, Frank Jülicher^{1,3,7¶}

Protein condensates are complex fluids that can change their material properties with time. However, an appropriate rheological description of these fluids remains missing. We characterize the time-dependent material properties of *in vitro* protein condensates using laser tweezer-based active and microbead-based passive rheology. For different proteins, the condensates behave at all ages as viscoelastic Maxwell fluids. Their viscosity strongly increases with age while their elastic modulus varies weakly. No significant differences in structure were seen by electron microscopy at early and late ages. We conclude that protein condensates can be soft glassy materials that we call Maxwell glasses with age-dependent material properties. We discuss possible advantages of glassy behavior for modulation of cellular biochemistry.

Membraneless compartments in cells exhibit various material properties adapted to their biological purpose. Some compartments such as P-granules and stress granules are liquid-like, as shown by fusion and rapid molecular rearrangements (1, 2). Others such as centrosomes are less dynamic and can exhibit properties of amorphous gels (3, 4). Dynamic solids such as microtubules also exist (5). The study of rheological properties of biological compartments provides important information about the nature of molecular interactions and about the emergent, collective behaviors of the constituent molecules.

Under certain conditions, a protein solution *in vitro* can phase-separate to form protein-dense droplets (6, 7). Such droplets can behave as liquids. However, in many cases, the dynamics of these liquid-like materials slow over time and behave more solid-like. This has been observed *in vitro* for a variety of evolutionarily distinct proteins involved in different biological functions (2, 3, 6–10) as well as *in vivo* (4, 9, 11–14). Such behavior has been termed hardening or aging (2, 10).

We can distinguish several ways in which a liquid could become more solid-like (15–17).

One way is gelation through the introduction of cross-links. When the cross-links reach a critical density, a connected polymer network is formed that extends through the whole system, and there is a sudden transition from a viscoelastic fluid to a solid (17, 18). Another way for a liquid to become more solid-like is found in glass-forming systems, such as soft pastes and entangled polymer systems, which do not reach thermodynamic equilibrium (16, 19–21). Glassy systems can be distinguished from gelation by the fact that there is no sudden change of material properties with age (18, 22). Gels and glasses are typically amorphous. Liquids can also become more solid-like by the formation of fibers or crystal-like aggregates such as amyloids (2, 23). Membraneless compartments in cells have been called condensates in part to emphasize their physical nature. However, in general, we do not understand their physical properties. Probing material properties of condensates requires understanding of the time-dependent rheology.

We began by characterizing the change in protein diffusion in condensates as a function of their age t_w (defined as time after formation of droplets), using fluorescence recovery after photobleaching (FRAP) (Fig. 1A and movie S1). Diffusion of nonbleached protein into the bleached region is a measure of molecular mobility. Figure 1B shows typical recovery curves at early and late age, for the *C. elegans* protein PGL-3 (fig. S1C) (24). At early age below 30 min, fluorescently labeled PGL-3 fluorescence recovers with a half-time of ~1 min. At age $t_w = 46$ hours, recovery is slow with a half-time of ~50 min (Fig. 1B). A second measure of dynamics is the coalescence time of two spherical condensates. Two condensates with liquid-like behavior merge into a final spherical condensate over a time that depends on the ratio of surface tension and viscosity (Fig. 1C) (1). After formation, coalescence of PGL-3 droplets occurs within 10 s, whereas at an age $t_w = 46$ hours, it takes tens of minutes (Fig. 1D and movie S2). Similar behaviors

were seen for four other proteins of the FUS family [FUS, EWSR1, DAZAP1, and TAF15 (10)] (Fig. 1, A and C; fig. S1, A and C; and Table 1). These results are similar to previously published data and demonstrate the aging behavior of a wide variety of protein condensates (2, 3, 6, 7, 9, 25).

To characterize the mechanism by which the material properties of condensates change between early and late times after their formation, we used both active (26) and passive microrheology. For active microrheology, condensates were deformed using two laser tweezers that acted on two beads linked to a droplet through attached protein (Fig. 1, E and F). Sinusoidal forces with a given frequency were exerted on one bead and the bead displacements were recorded, which served as a measure of droplet deformation (Fig. 2A). At an early age, the force-displacement curve is an ellipse showing a strong viscous component. At a later age, the force-displacement curve is almost a straight line indicative of predominantly elastic behavior (Fig. 1G). For passive microrheology, we followed the movement of fluorescent polystyrene beads immersed in droplets using a confocal microscope (Fig. 1H and movie S3) (27, 28). We noticed that droplets decreased their size as they age (Fig. 1H). Furthermore, at early age, the diffusive bead motion reached larger distances as compared with later ages within the same time window (Fig. 1I). Despite the changes in material properties and droplet size for PGL-3 and FUS, cryo-electron tomography showed no detectable changes in structural features inside the drops, and the material appeared amorphous at all times. Occasional fibrous structures existed at the surface of late FUS droplets but not in the bulk (fig. S1B).

To further investigate the material properties, we measured the frequency-dependent complex shear modulus $G^* = G' + iG''$ as a function of the droplet age t_w after droplet formation using active microrheology (26). The storage modulus G' characterizes the elastic response of the droplets, and the loss modulus G'' characterizes the viscous component of the response. For PGL-3, at early ages and for low frequencies ω , the loss modulus is larger than the storage modulus, indicating predominantly liquid-like behavior (Fig. 2B, blue symbols). At high frequencies, the elastic modulus surpasses the loss modulus, indicating that at these frequencies, the mechanical response is predominantly elastic. The crossing-over between predominantly elastic and predominantly viscous behaviors occurs at the angular frequency ω_c . At this frequency, the storage modulus G' equals the loss modulus G'' . The crossover frequency ω_c decreased as the sample aged (Fig. 2C, red symbols). The frequency-dependent responses obtained at early and late waiting times were different. However,

¹Max Planck Institute for the Physics of Complex Systems, Nöthnitzer Str. 38, 01187 Dresden, Germany. ²Max Planck Institute of Molecular Cell Biology and Genetics, Pfotenhauerstraße 108, 01307 Dresden, Germany. ³Cluster of Excellence Physics of Life, Technische Universität Dresden, Dresden, Germany. ⁴Biotec, TU Dresden, Tatzberg 47-49, 01307 Dresden, Germany. ⁵EMBL Heidelberg, Meyerhofstraße 1, 69117 Heidelberg, Germany. ⁶Institute of Molecular Biotechnology of the Austrian Academy of Sciences (IMBA), Vienna BioCenter (VBC), Dr. Bohrgasse 3, 1030 Vienna, Austria. ⁷Center for Systems Biology Dresden, Pfotenhauerstr. 108, 01307 Dresden, Germany.

*Present address: Max Planck Institute for Dynamics and Self-Organization, Am Faßberg 17, 37077 Göttingen, Germany.

†Present address: Whitehead Institute for Biomedical Research 455 Main St, Cambridge, MA 02142, USA.

‡Present address: Max Planck Institute of Biophysics, Max-von-Laue-Straße 3, 60438 Frankfurt am Main, Germany.

§Present address: ETH Zürich, Vladimir-Prelog-Weg 1-5/10, 8093 Zürich, Switzerland.

¶Corresponding author. Email: hyman@mpi-cbg.de (A.A.H.); julicher@pks.mpg.de (F.J.)

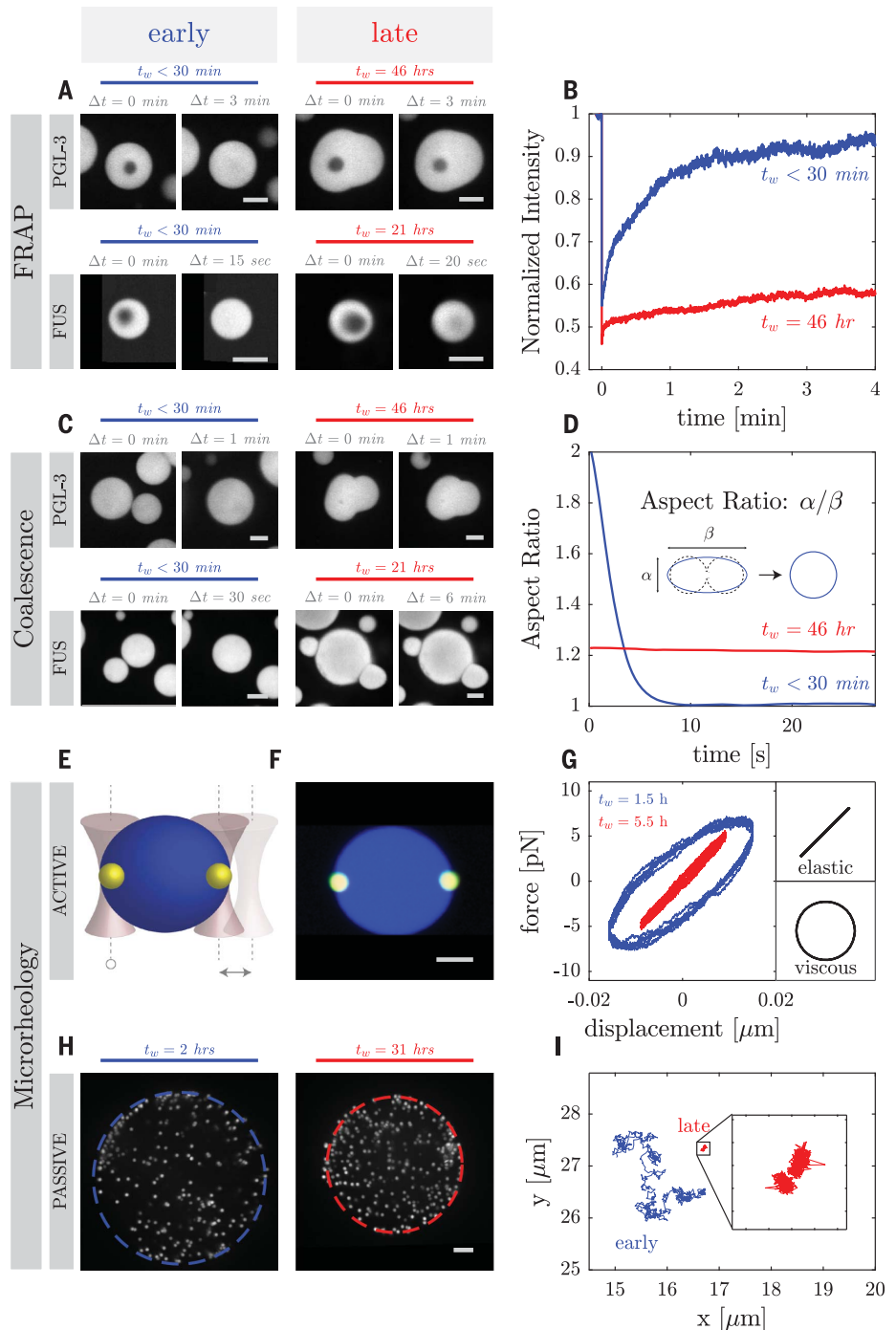
they are both well described by a Maxwell fluid albeit with different characteristic relaxation times τ_C (Fig. 2, B and C, gray lines). For a Maxwell fluid the crossover frequency is $\omega_C = 1/\tau_C$, where τ_C is the Maxwell relaxation time. The time scale τ_C characterizes the droplet response to a deformation: For deformations on time scales shorter than τ_C , the droplet response is primarily elastic, whereas for deformations on time scales longer than τ_C , the response is primarily viscous and the droplet will flow. Therefore, our active microrheology

data show that as the system ages, the time scale τ_C increases, indicating that the droplet exhibits elastic behaviors over an increasingly broad range of frequencies, corresponding to droplet aging. The scaling of frequency-dependent complex moduli is revealed by plotting the data with respect to a rescaled frequency axis. The data for different ages of PGL-3 droplets collapse on a single curve, which matches the behavior of a simple Maxwell fluid closely (Fig. 2D). We also performed active microrheology on protein condensates com-

posed of FUS protein and again found rheology consistent with a Maxwell fluid. We repeated our measurements on PGL-3 under buffer conditions with varying salt concentrations (fig. S3, A to C) and with different temperatures (fig. S3, F to H, and supplementary materials). These data reveal that with increased temperature or increased salt concentration, droplet aging slows and droplets appear liquid-like for a longer period of time. At a late age, an additional short-time viscosity λ can be identified, which becomes

Fig. 1. Protein droplets exhibit age-dependent material properties.

We compare the properties of droplets shortly after formation ($t_w = 0$ min, early droplets) with droplets observed after a time t_w of several hours of formation (late droplets). **(A)** FRAP of protein droplets composed of PGL-3-GFP and FUS-GFP, respectively. Shown are images of early and late droplets immediately after bleaching ($\Delta t = 0$ min) as well as after a time Δt after bleaching. **(B)** Fluorescence intensity of the photobleached area for the PGL-3-GFP droplets shown in (A) for both early (blue) and late (red) droplets. **(C)** Images of FUS-GFP and PGL-3-GFP droplets undergoing coalescence. Shown are images at the time of contact $\Delta t = 0$ as well as at a time Δt after coalescence. **(D)** Aspect ratio of the coalescing PGL-3-GFP droplets shown in (C) is shown as a function of time for early (blue) and late (red) droplets. The aspect ratio is defined as the ratio of the major to minor axes of a representative ellipse. **(E)** Schematic representation of the dual optical trap active microrheology experiment. Polystyrene beads are shown in yellow, and the droplet is shown in blue. One trap is fixed, and one trap oscillates. **(F)** Confocal image of a PGL-3-GFP droplet with two 2 μm -diameter beads in a dual optical trap. **(G)** Lissajous plot of force versus trap displacement for an early (blue) PGL-3 droplet indicating viscous behavior. The plot for the late (red) droplet indicating elastic behavior. **(H)** Confocal images of the midsection of a large PGL-3 droplet containing 1 μm -diameter fluorescent polystyrene beads early (blue) and late (red) after droplet formation. **(I)** Two examples of trajectories over 3 hours of embedded beads in a PGL-3 droplet, early (blue, $t_w = 3$ hours) and late (red, $t_w = 36$ hours) after droplet formation (length of inset box represents 0.5 μm). Scale bars in all panels represent 5 μm .



relevant at high frequencies and does not change significantly with age. This can be described by a Jeffreys fluid model (supplementary materials and fig. S8) (29). We determine λ values between 6 mPa·s and 1.3 Pa·s, which we attribute to the solvent. For FUS protein, we also observe an age-independent high-frequency viscosity in the same range (Fig. 4B and fig. S8, B and C). We conclude that at all conditions, the droplets exhibit Maxwell fluid rheology with age-dependent relaxation time.

Fig. 2. Active rheology of early and late PGL-3 droplets.

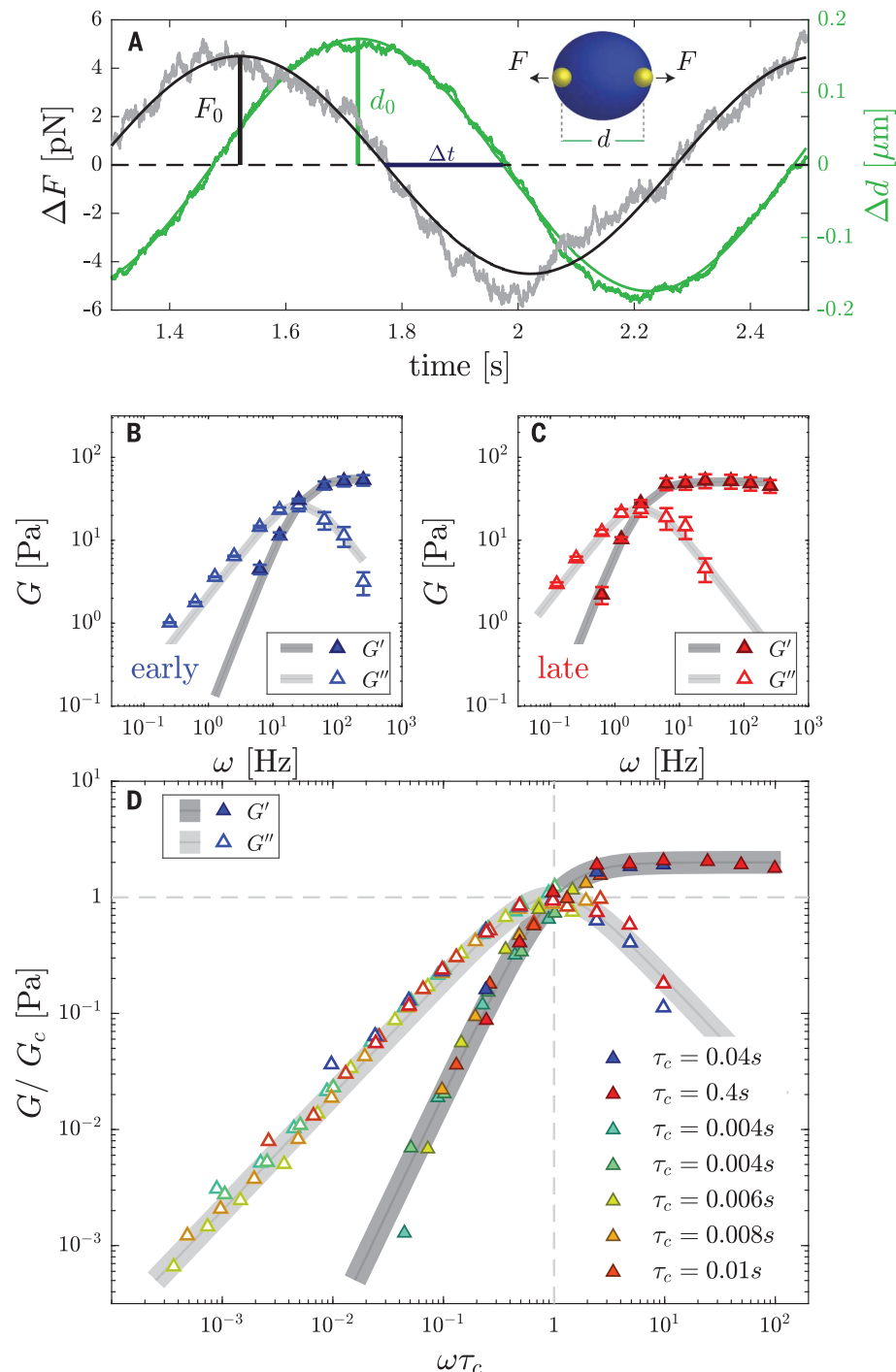
A droplet is trapped between two beads using a dual optical trap; one trap is undergoing oscillatory displacement while the other trap is at a fixed position. (A) Force ΔF is shown as a function of time (gray) together with a sinusoidal fit (black solid line). The corresponding droplet deformation Δd (green) is shown together with a sinusoidal fit (solid green line). We determine the force amplitude F_0 , the deformation amplitude d_0 , and the phase shift $\varphi = \omega\Delta t$ from the fits where ω is the imposed angular frequency. (B) Storage and loss moduli, G' and G'' , are shown as a function of frequency for an early droplet ($t_w = 0.5$ hours with a surface tension of 4.5 $\mu\text{N/m}$). The corresponding frequency-dependent moduli of a Maxwell element with a characteristic time scale $\tau_c = 0.039$ s and plateau modulus $E = 56$ Pa are shown in gray. Error bars represent measurement uncertainty (supplementary materials). (C) Same plot as in (B) for the same droplet late after formation ($t_w = 1.5$ hours with a surface tension of 19.3 $\mu\text{N/m}$). The complex elastic modulus of a Maxwell element with a characteristic time scale $\tau_c = 0.39$ s and plateau modulus $E = 50.7$ Pa is shown in gray. Error bars represent measurement uncertainty (supplementary materials). (D) Scaled storage and loss moduli, G'/G_c and G''/G_c , are plotted as a function of scaled frequency $\omega\tau_c$ for the droplets shown in (B) and (C) (blue, red) and additional droplets (colors indicate characteristic time τ_c). G_c is the crossover modulus. A scaled Maxwell fluid is shown in gray. For all panels, the storage moduli G' are shown as solid triangles, and the loss moduli G'' are shown as open triangles. (B to D) Droplets were formed in a solution with a final KCl concentration of 75 mM.

Using passive microrheology, we measured the mean square displacement over time of beads immersed in the droplets (Figs. 1H and 3A and supplementary materials). We were concerned that the change in droplet radius would contribute to the mean square displacement of beads. Therefore, we first measured the droplet radius as a function of time (Fig. 3B, orange line). Droplet shrinking can also be estimated on the basis of net particle motion (Fig. 3, A and B, blue line). These two measures show good agreement, with small discrep-

ancies at later ages (Fig. 3B, fig. S5A, and supplementary materials). The average particle displacement is proportional to distance from the droplet center, indicating that the droplet is shrinking uniformly in space (Fig. 3A). We quantified the mean square displacement

$$\langle \Delta r(\tau, t_w)^2 \rangle = \langle [r(t_w + \tau) - r(t_w)]^2 \rangle \quad (1)$$

of the beads over time τ for different droplet ages t_w , where r is the bead position in the image plane, after contributions from droplet



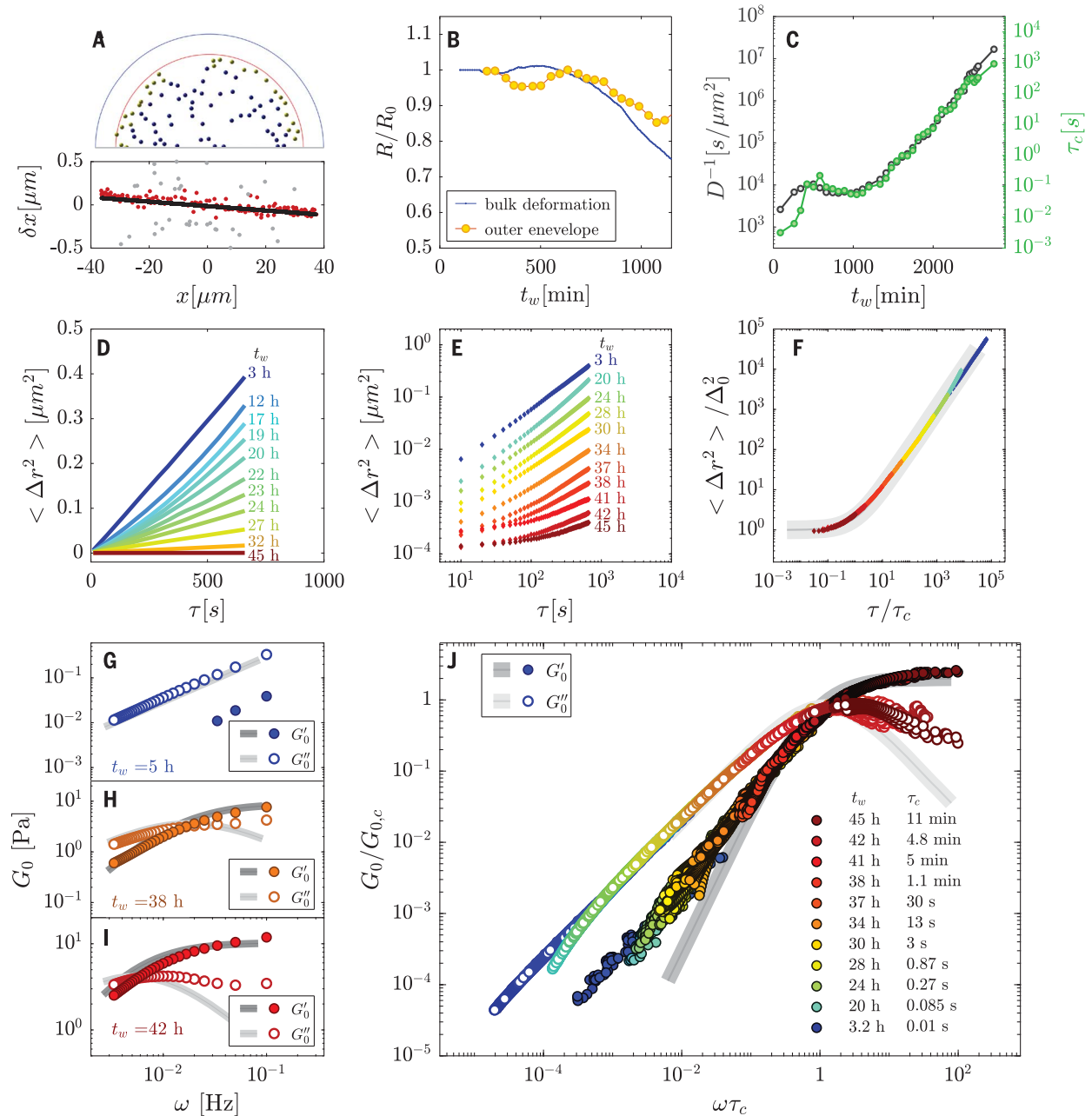


Fig. 3. Passive microrheology of early and late PGL-3 droplets. (A) Image of particles representing bead positions in the upper half of a droplet several hours after formation ($t_w = 27$ hours). Beads in yellow are considered boundary particles and are not considered for bead-diffusion analysis. The blue outline represents the droplet border shortly after droplet formation; the red outline represents the droplet border at $t_w = 27$ hours. Particle displacements δx in the x direction resulting from droplet shrinkage are shown below for a time interval of $\tau = 2.5$ min at droplet age $t_w = 8$ hours plotted with respect to x position in the droplet. The slope of these particle displacements determined by a linear fit (black line) characterizes average particle motion due to droplet shrinkage. Data points within a standard deviation of the linear fit are shown in red, the remaining ones in gray. (B) Scaled droplet radius, R/R_0 , is shown as a function of droplet age t_w , where R_0 is the initial droplet radius (orange). The scaled radius inferred from average particle displacements is shown in blue (supplementary materials). (C) Inverse of the diffusion coefficient D^{-1} of embedded beads calculated from the mean square displacement during $\tau = 20$ min is shown as a function of waiting time t_w . The characteristic relaxation time τ_c is shown in green. (D) Mean square displacement $\langle \Delta r^2 \rangle$ as a function of lag time τ shown for different

waiting times t_w . (E) Double logarithmic plot of $\langle \Delta r^2 \rangle$ as a function of lag time τ for different waiting times t_w . (F) Plot of normalized mean square displacement, $\langle \Delta r^2 \rangle / \Delta_0^2$, as a function of normalized lag time τ/τ_c , where Δ_0^2 is the offset and τ_c is a characteristic time. The values of τ_c that correspond to the mean square displacements shown in (E) are chosen such that the data for different waiting times t_w collapse onto a single curve, which is well described by $\langle \Delta r^2 \rangle = \Delta_0^2 \left(1 + \frac{\tau}{\tau_c}\right)$ (gray line).

(G to I) Real and imaginary parts, G'_0 and G''_0 , of the inferred complex shear moduli G_0^* for waiting times $t_w = 5$ hours (G), 38 hours (H), and 42 hours (I) (supplementary materials). (J) Normalized inferred shear moduli as a function of the normalized frequency $\omega\tau_c$ for all measurements of mean square displacement. The colors indicate the waiting time t_w , and the color code is the same as in (D) and (E). In addition, the value of characteristic times τ_c is indicated. The values of $G_{0,c}$ are inferred from the fit in (F) using the relationship $G_{0,c} = k_B T / (3\pi a \Delta_0^2)$. Inferred shear moduli shown in (G) to (J) were approximated using Eq. 14 of the supplementary materials. The gray lines in (G) to (J) correspond to the inferred complex moduli for a single-relaxation-time Maxwell fluid using the same approximation.

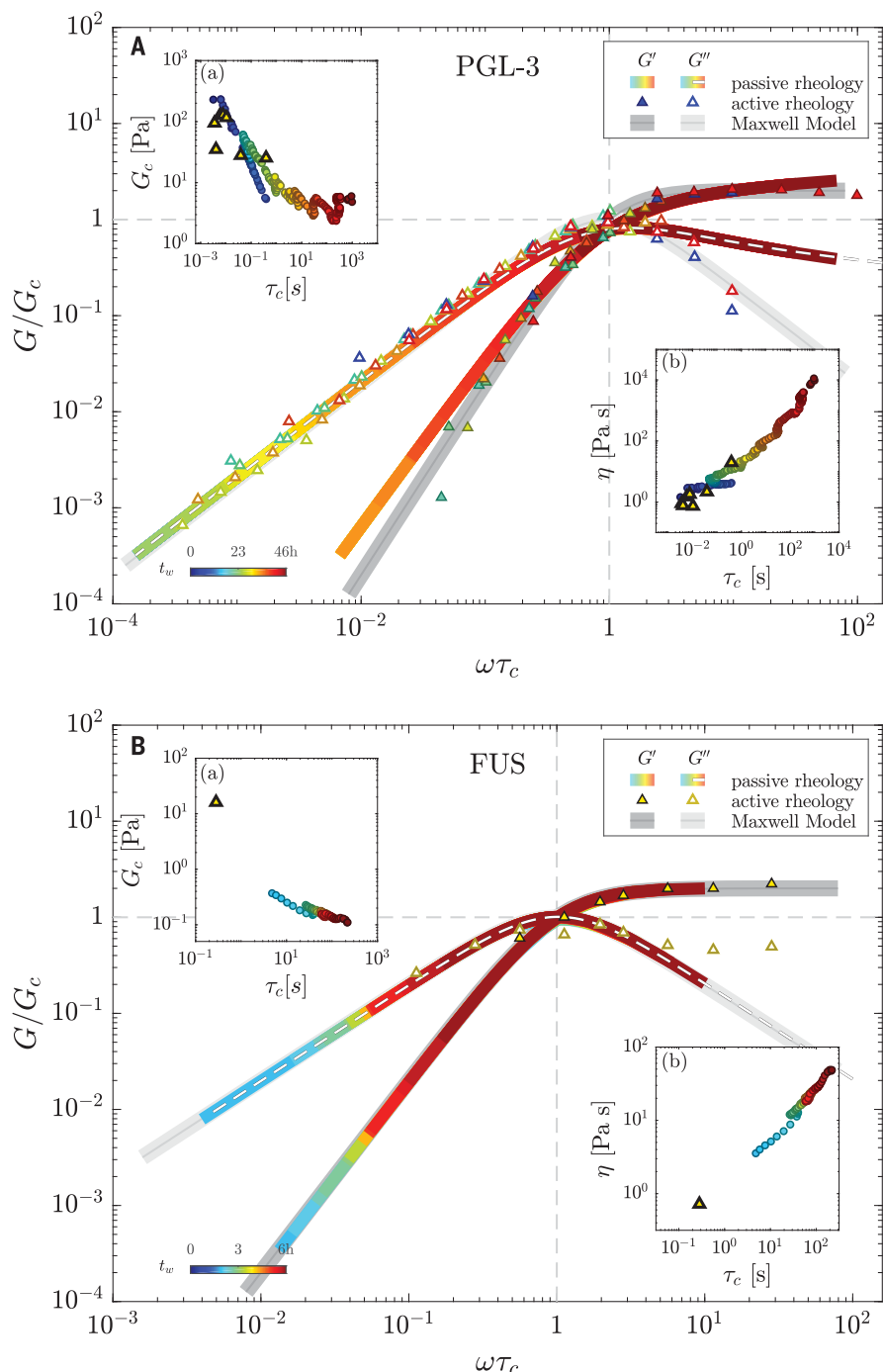


Fig. 4. Dimensionless loss and storage moduli obtained by active and passive microrheology collapse onto single curves. (A) Shear moduli G and G_0 scaled by the respective crossover moduli G_c and $G_{0,c}$ plotted as a function of dimensionless frequency $\omega\tau_c$. The active microrheology data are shown in open and solid triangles. The moduli inferred from passive microrheology as shown solid colored lines. These lines were obtained using passive microrheology data (Fig. 3F and supplementary materials). For active and passive microrheology, the same color code as in Figs. 2, B to D, and 3, E to J, is used. The thick gray lines represent the frequency response of a Maxwell fluid. (Inset a) Crossover moduli for active and passive microrheology G_c (yellow triangles) and $G_{0,c}$ (colored circles), respectively, are plotted as a function of characteristic time, τ_c . (Inset b) Viscosities for active and passive microrheology $\eta = 2G_c\tau_c$ (yellow triangles) and $\eta_0 = 2G_{0,c}\tau_c$ (colored circles), respectively, are plotted as a function of characteristic time, τ_c . Shear moduli inferred from passive microrheology were obtained using Eq. 18 of the supplementary materials. The gray lines correspond to the complex moduli of a single-relaxation-time Maxwell fluid. PGL-3 droplets were formed in a solution with a final KCl concentration of 75 mM. (B) Plot analogous to the upper plot with active and passive microrheology of FUS protein. FUS droplets were formed in a solution with final KCl concentrations of 75 mM and 250 mM for passive and active droplets, respectively.

shrinkage have been subtracted. We also corrected for the noise floor because of experimental noise (supplementary materials and fig. S7). The angle brackets denote an average over beads and over an age window of 1 hour (supplementary materials). We found that at early ages t_w , the mean square displacement increases linearly with time τ and reaches $\sim 0.4 \mu\text{m}^2$ within 10 min (Fig. 3, D and E, blue lines). For increasing droplet ages, the slope of the mean square displacement decreases (Fig. 3, D and E). The diffusivity can be determined through the slope of the mean square displacement as a function of time $\langle \Delta r^2(\tau, t_w) \rangle \approx \Delta_0^2 + 4D(t_w)\tau$, where Δ_0^2 is an offset that is independent of τ but can depend on age t_w . $D(t_w)$ is an age-dependent effective diffusivity; inverse $D(t_w)$ is shown in Fig. 3C, black line. As the system ages, $D(t_w)$ decreases steadily but remains almost constant with $D \approx 10^{-4} \mu\text{m}^2/\text{s}$ for t_w less than ~ 1000 min (15 hours). For passive, equilibrated samples, this value corresponds to a viscosity of ~ 1 Pa·s, which is consistent with previous estimates of PGL-3 droplet viscosity (26, 28). For ages t_w greater than 1000 min, $D(t_w)$ decreases with age and reaches a value of $D \approx 1.5 \cdot 10^{-7} \mu\text{m}^2/\text{s}$ at ~ 2500 min (Fig. 3C). For passive liquids, this corresponded to a viscosity of $\sim 10^3$ Pa·s. When the mean square displacement curves are examined on a logarithmic scaling, the curve reaches a finite value at low τ , indicative of an elastic regime (Fig. 3, E and F). Consistent with the active microrheology, the mean square displacement data collapse to a single curve well described by a Maxwell fluid, when rescaling the time τ and $\langle \Delta r^2 \rangle$ by the age-dependent relaxation time τ_c and the offset Δ_0^2 (Fig. 3, D to F, and supplementary materials).

Passive microrheology assesses fluid properties from mean square displacement measurements using the fluctuation-dissipation relation (27, 30). The fluctuation-dissipation relation applies to equilibrium systems. However, an aging system has not reached equilibrium. We reasoned that for sufficiently short time scales compared with the age t_w quasi-equilibrium of many degrees of freedom may hold (31), and the fluctuation-dissipation relation may provide useful estimates of material properties. We therefore determined the frequency-dependent complex shear modulus $G_0^* = G_0' + iG_0''$ inferred from the fluctuation-dissipation relation using the mean square displacement data (supplementary materials). The moduli G_0 obtained this way qualitatively exhibit the frequency-dependent behaviors of a Maxwell fluid with age-dependent Maxwell times (Fig. 3, G to I). The frequency-dependent moduli $G_0(\omega)$ as a function of frequency at different age t_w collapse on a single curve when the frequency axis is scaled with the time τ_c and the moduli are scaled by the value $G_{0,c}$, defined as the value of the real and imaginary parts of G_0^* at the point where both are equal

(Fig. 3J). Consistent with the active microrheology data, the passive microrheology data also exhibit at all ages the qualitative behaviors of a Maxwell fluid (compare Fig. 2D with Fig. 3J). We also performed passive microrheology on protein condensates composed of FUS protein and PGL-3–green fluorescent protein (GFP) (figs. S5 and S6). Our bead-tracking measurements on these condensates again reveal at all ages the qualitative properties of a single-time Maxwell fluid.

We highlight the similarity of active and passive microrheology by plotting the scaled shear moduli as a function of scaled frequency for both active (triangles) and passive (colored lines) microrheology in the same plot for both PGL-3 and FUS proteins (Fig. 4). The data collapse and are well captured by a single-time Maxwell fluid (Fig. 4, gray lines). When examining the moduli G_C , obtained for active microrheology taken from many aging droplets, we find values that vary over approximately one order of magnitude [Fig. 4, A and B, insets (a), yellow triangles]. The values of $G_{0,C}$ obtained by passive microrheology for one aging droplet exhibit a trend toward smaller values for larger τ_C [Figs. 3, G to I, and 4A, inset (a), colored circles]. We also estimated the long time viscosities, $\eta = 2G_C\tau_C$ and $\eta_0 = 2G_{0,C}\tau_C$, for active and passive microrheology, respectively [Fig. 4A, inset (b)]. The viscosity strongly increases with τ_C , and both active and passive microrheology share the same trend. To compare the inferred moduli determined by the active and passive microrheology, we define the ratio $\xi = \langle G_C \rangle / \langle G_{C,0} \rangle$, where brackets denote the average over several droplets and several values of τ_C . Using the window of $0.004 \text{ s} < \tau_C < 0.442 \text{ s}$, we find $\xi \approx 2.63 \pm 2.57$. One can interpret ξ as an effective noise strength that replaces the amplitude of fluctuations in the fluctuation-dissipation relation (32–35). The product ξT is sometimes called an effective temperature. This suggests that the fluctuation-dissipation relation is only weakly violated, at least, at early ages similar to previous reports on soft glasses (32, 36). Our data further show that the elastic modulus does not tend to increase with time, suggesting that the term

hardening is not appropriate for the change in material properties of condensates consisting of PGL-3 and FUS family proteins. Rather, we use the term aging.

A defining and unexpected rheological feature of the condensates we study is the self-similarity of their material properties as they age. This self-similarity is manifested by the fact that at all ages, they exhibit the same viscoelastic behavior of a Maxwell fluid. An ordinary Maxwell fluid does not age and reaches a thermodynamic equilibrium because it has a fixed relaxation time. However, the relaxation time of the protein condensates in this study increases with age. Age-dependent relaxation times are typical for glass-forming systems. We thus refer to a Maxwell fluid with age-dependent relaxation time as a Maxwell glass (supplementary materials). Our data suggest that the molecular components increasingly interact and lose their freedom to move as the condensates shrink and their density increases. Such behaviors are also seen in other glass-forming systems (15, 16, 37–40). The dependence of aging characteristics on salt concentration that we observe suggests that electrostatic interactions play a role in the aging of protein condensates (41).

A key question will be to relate glassy behavior to molecular configurations. The associative polymer ideas of Semenov and Rubenstein are a beautiful and elegant way to understand viscoelastic and Maxwell-like behaviors of polymer systems and describe the equilibrium properties and kinetics of such systems (42). However, they do not address aging. An example of how dynamics can slow is jamming (43). However, this is a simplified picture based on excluded volume and rigid objects such as spherical particles. For condensate-forming proteins, a more appropriate picture may be based on the fact that these proteins have large regions of disorder (6). Disordered proteins can take many different molecular configurations leading to complex energy landscapes with distributions of energy minima (44). Increasing relaxation times are likely related to the system exploring deeper energy minima that are increasingly inaccessible, but longer lived,

as the system ages (45–47). Such ideas have been put forward in the context of protein folding (44, 48, 49) but still need to be explored in the context of higher-order protein assemblies.

In conclusion, we provide evidence that biological condensates made from a variety of proteins can best be described as Maxwell glasses. At any particular age, the rheology reveals the expected viscoelastic properties of a Maxwell fluid, well described by a single relaxation time. However, at different ages, the relaxation times themselves are different. Therefore, the term Maxwell glass incorporates the aging of Maxwell fluids and glasses. The role of glass-like behaviors have not been well characterized in biology, which has tended to stress gel-like characteristics of biological materials (7, 50). This is because glass-like aging is a dynamic process and, therefore, more difficult to study because it requires a broad range of time scales. However, glass-like behavior offers a number of interesting possibilities for cellular function compared with a gel-like state. A soft gel will either respond elastically or break under stress and tends to require chemical modification for disassembly. On the other hand, because glasses can start to flow when mechanically stressed (51), glass-like soft pastes offer a tension sensor to cells that can couple mechanical stresses to biochemistry. The nature of glass-like states makes it easy to fluidize a biological glass simply by changing composition, temperature, or salt concentration. More generally, soft glasses allow cells to slow down biochemistry while maintaining a soft material, which can flexibly and rapidly respond to changing conditions. Little is known about the relationship between pathology and stiffness of aggregates, but stiffer structures likely could be more disruptive to the mechanical environment of a cell. Cells in tissues are constantly responding to mechanical perturbation from other cells in the tissue and must be able to respond as soft materials. Glass-like aging of protein condensates may, therefore, offer cells a way to flexibly modulate mechanical properties of membraneless organelles while allowing for rapid response to changing environmental cues.

Table 1. Characteristics of the proteins used in this study. The first four proteins are from the FUS family. Protein length is reported in number of amino acids. All molecular weights and sequence lengths are reported for untagged proteins. The addition of a GFP tag adds 29 to 31 kDa in molecular weight and 260 to 278 amino acids in length. The GFP tag is on the N terminus for DAZAP1, whereas all other proteins have the GFP tag on the C terminus.

Protein name	Length	Molecular weight [Da]	Plasmid name	Virus number	Gene
DAZAP1	407	43,384	TH1272	1424	DAZAP1
EWSR1	656	68,480	TH1259	1510	EWSR1
FUS	526	53,426	TH1204	3311	FUS
TAF15	589	61,559	TH1258	1480	TAF15
PGL-3	693	74,700	pSS2B	1522	PGL3

REFERENCES AND NOTES

- C. P. Brangwynne *et al.*, *Science* **324**, 1729–1732 (2009).
- A. Patel *et al.*, *Cell* **162**, 1066–1077 (2015).
- J. B. Woodruff *et al.*, *Cell* **169**, 1066–1077.e10 (2017).
- M. Mittasch *et al.*, *J. Cell Biol.* **219**, e201912036 (2020).
- A. Desai, T. J. Mitchison, *Annu. Rev. Cell Dev. Biol.* **13**, 83–117 (1997).
- S. F. Banani, H. O. Lee, A. A. Hyman, M. K. Rosen, *Nat. Rev. Mol. Cell Biol.* **18**, 285–298 (2017).
- Y. Shin, C. P. Brangwynne, *Science* **357**, eaaf4382 (2017).
- Y. Lin, D. S. Protter, M. K. Rosen, R. Parker, *Mol. Cell* **60**, 208–219 (2015).
- T. M. Franzmann *et al.*, *Science* **359**, eaao5654 (2018).
- J. Wang *et al.*, *Cell* **174**, 688–699.e16 (2018).
- A. R. Strom *et al.*, *Nature* **547**, 241–245 (2017).
- K. E. Kistler *et al.*, *eLife* **7**, e37949 (2018).
- S. J. Nair *et al.*, *Nat. Struct. Mol. Biol.* **26**, 193–203 (2019).
- S. Jang *et al.*, *Biophys. J.* S0006-3495(20)30597-X (2020).
- J. M. Hutchinson, *Prog. Polym. Sci.* **20**, 703–760 (1995).
- C. B. Roth, *Polymer Glasses* (CRC, 2016).
- M. Rubinstein, R. H. Colby, *Polymer Physics*, vol. 23 (Oxford Univ. Press, 2003).
- H. H. Winter, M. Mours, in *Neutron Spin Echo Spectroscopy Viscoelasticity Rheology*, vol. 134 of *Advances in Polymer Science* (Springer, 1997), pp. 165–234.
- L. Berthier, G. Biroli, *Rev. Mod. Phys.* **83**, 587–645 (2011).
- H. Lindsay, P. Chaikin, *J. Chem. Phys.* **76**, 3774–3781 (1982).
- A. Ikeda, L. Berthier, P. Sollich, *Soft Matter* **9**, 7669 (2013).
- A. S. Negi, C. G. Redmon, S. Ramakrishnan, C. O. Osuji, *J. Rheol.* **58**, 1557–1579 (2014).
- M. Kato *et al.*, *Cell* **149**, 753–767 (2012).
- S. Saha *et al.*, *Cell* **166**, 1572–1584.e16 (2016).
- S. Maharana *et al.*, *Science* **360**, 918–921 (2018).
- L. M. Jawerth *et al.*, *Phys. Rev. Lett.* **121**, 258101 (2018).
- M. L. Gardel, M. T. Valentine, D. A. Weitz, *Microrheology* (Springer, 2005).
- S. Elbaum-Garfinkle *et al.*, *Proc. Natl. Acad. Sci. U.S.A.* **112**, 7189–7194 (2015).
- Y. L. Raikher, V. V. Rusakov, R. Perzynski, *Soft Matter* **9**, 10857 (2013).
- T. G. Mason, *Rheol. Acta* **39**, 371–378 (2000).
- L. C. E. Struik, thesis, Technische Hogeschool Delft (1977).
- S. Jabbari-Farouji *et al.*, *Europhys. Lett.* **84**, 20006 (2008).
- L. Cipelletti, L. Ramos, *J. Phys. Condens. Matter* **17**, R253–R285 (2005).
- L. F. Cugliandolo, J. Kurchan, L. Peliti, *Phys. Rev. E* **55**, 3898–3914 (1997).
- L. F. Cugliandolo, *J. Phys. A* **44**, 483001 (2011).
- B. Abou, F. Gallet, *Phys. Rev. Lett.* **93**, 160603 (2004).
- R. L. Moorcroft, M. E. Cates, S. M. Fielding, *Phys. Rev. Lett.* **106**, 055502 (2011).
- C. Derec, A. Ajdari, F. Lequeux, *Eur. Phys. J. E* **4**, 355–361 (2001).
- G. B. McKenna, S. L. Simon, in *Polymer Glasses* (CRC, 2016), pp. 39–70.
- B. Ruzicka, E. Zaccarelli, *Soft Matter* **7**, 1268 (2011).
- J. van der Gucht, E. Spruijt, M. Lemmers, M. A. Cohen Stuart, *J. Colloid Interface Sci.* **361**, 407–422 (2011).
- M. Rubinstein, A. N. Semenov, *Macromolecules* **34**, 1058–1068 (2001).
- A. J. Liu, S. R. Nagel, *Annu. Rev. Condens. Matter Phys.* **1**, 347–369 (2010).
- Y. Chebaro, A. J. Ballard, D. Chakraborty, D. J. Wales, *Sci. Rep.* **5**, 10386 (2015).
- J. P. Bouchaud, *J. Phys. I* **2**, 1705–1713 (1992).
- P. Sollich, F. Lequeux, P. Hébraud, M. E. Cates, *Phys. Rev. Lett.* **78**, 2020–2023 (1997).
- C. Monthus, J.-P. Bouchaud, *J. Phys. Math. Gen.* **29**, 3847–3869 (1996).
- J. N. Onuchic, Z. Luthey-Schulten, P. G. Wolynes, *Annu. Rev. Phys. Chem.* **48**, 545–600 (1997).
- S.-H. Chong, S. Ham, *Sci. Rep.* **9**, 14927 (2019).
- M. Hondele, S. Heinrich, P. De Los Rios, K. Weis, *Emerg. Top. Lif. Sci.* (2020).
- M. Cloitre, R. Borrega, L. Leibler, *Phys. Rev. Lett.* **85**, 4819–4822 (2000).

ACKNOWLEDGMENTS

We thank the members of MPI-CBG and MPI-PKS for useful discussions; in particular, we thank C. Duclut, P. McCall, S. Muenster,

L. Hubatsch, T. Harmon, and C. Weber. We also thank B. Schroth-Diez, J. Peychl, and the light microscopy facility as well as R. Lemaître and the protein expression facility at the MPI-CBG. **Funding:** This project was supported by funding from the Max Planck Society. A.A.H. was funded by the Deutsche Forschungsgemeinschaft (DFG, German Research Foundation) (ZE1216/1-1; HY3/6-1). A.A.H., F.J., and E.F.-F. were supported by the Deutsche Forschungsgemeinschaft (DFG, German Research Foundation) under Germany's Excellence Strategy (EXC-2068; 390729961) Cluster of Excellence Physics of Life of TU Dresden. J.M. acknowledges funding from EMBL and the European Research Council (760067). **Author contributions:** L.J., A.A.H., and F.J. designed and coordinated the study. L.J. performed experimental work, image processing, and data analysis. E.F.-F. performed optical tweezer data analysis. L.J., E.F.-F., F.J., A.A.H., and Su.S. performed theoretical work. Sh.S., M.R., and J.W. provided proteins and reagents. M.I. performed initial optical tweezer experiments. T.F., X.Z., J.S., and J.M. performed cryo-electron microscopy experiments. All authors contributed to data analysis and interpretation. **Competing interests:** A.A.H. is a co-founder and SAB member of Dewpoint therapeutics. A.A.H. is also a co-founder of Caraway therapeutics. **Data and materials availability:** All data needed to evaluate the conclusions in the paper are present in the paper or the supplementary materials.

SUPPLEMENTARY MATERIALS

science.sciencemag.org/content/370/6522/1317/suppl/DC1
Materials and Methods
Supplementary Text
Figs. S1 to S9
References (52–59)
Movies S1 to S3

[View/request a protocol for this paper from Bio-protocol.](#)

5 February 2019; resubmitted 18 June 2019
Accepted 16 October 2020
10.1126/science.aaw4951

Protein condensates as aging Maxwell fluids

Louise Jawerth, Elisabeth Fischer-Friedrich, Suropriya Saha, Jie Wang, Titus Franzmann, Xiaojie Zhang, Jenny Sachweh, Martine Ruer, Mahdiye Ijavi, Shambaditya Saha, Julia Mahamid, Anthony A. Hyman and Frank Jülicher

Science **370** (6522), 1317-1323.
DOI: 10.1126/science.aaw4951

Rheology of aging protein condensates

Protein condensates that form by undergoing liquid-liquid phase separation will show changes in their rheological properties with time, a process known as aging. Jawerth *et al.* used laser tweezer-based active and microbead-based passive rheology to characterize the time-dependent material properties of protein condensates (see the Perspective by Zhang). They found that condensate aging is not gelation of the condensates, but rather a changing viscoelastic Maxwell liquid with a viscosity that strongly increases with age, whereas the elastic modulus stays the same.

Science, this issue p. 1317; see also p. 1271

ARTICLE TOOLS

<http://science.sciencemag.org/content/370/6522/1317>

SUPPLEMENTARY MATERIALS

<http://science.sciencemag.org/content/suppl/2020/12/09/370.6522.1317.DC1>

RELATED CONTENT

<http://science.sciencemag.org/content/sci/370/6522/1271.full>

REFERENCES

This article cites 53 articles, 6 of which you can access for free
<http://science.sciencemag.org/content/370/6522/1317#BIBL>

PERMISSIONS

<http://www.sciencemag.org/help/reprints-and-permissions>

Use of this article is subject to the [Terms of Service](#)

Science (print ISSN 0036-8075; online ISSN 1095-9203) is published by the American Association for the Advancement of Science, 1200 New York Avenue NW, Washington, DC 20005. The title *Science* is a registered trademark of AAAS.

Copyright © 2020 The Authors, some rights reserved; exclusive licensee American Association for the Advancement of Science. No claim to original U.S. Government Works